gr-qc 0910.3656

The Asymptotic Falloff of Local Waveform Measurements in Numerical Relativity

Denis Pollney,[1] Christian Reisswig,[1] Nils Dorband,[1] Erik Schnetter,[2,3] and Peter Diener[3,2]

[1] *Max-Planck-Institut für Gravitationsphysik, Albert-Einstein-Institut, Potsdam-Golm, Germany*
[2] *Center for Computation & Technology, Louisiana State University, Baton Rouge, LA, USA*
[3] *Department of Physics & Astronomy, Louisiana State University, Baton Rouge, LA, USA*

(Dated: October 19, 2009)

We examine current numerical relativity computations of gravitational waves, which typically determine the asymptotic waves at infinity by extrapolation from finite (small) radii. Using simulations of a black hole binary with accurate wave extraction at $r = 1000M$, we show that extrapolations from the near-zone are self-consistent in approximating measurements at this radius, although with a somewhat reduced accuracy. We verify that ψ_4 is the dominant asymptotic contribution to the gravitational energy (as required by the peeling theorem) but point out that gauge effects may complicate the interpretation of the other Weyl components.

PACS numbers: 04.25.dg, 04.30.Db, 04.30.Tv, 04.30.Nk

arXiv:0910.3656v1 [gr-qc] 19 Oct 2009

I. Introduction. – Numerical relativity has made great strides in recent years in the solution of the binary black hole (BH) problem. Since the original breakthroughs by Pretorius [1] and the moving puncture approach [2, 3], the calculation of long, accurate gravitational waveforms (GWs) has become an almost routine procedure. It is particularly satisfying that a variety of methods (numerical methods, formulations of the Einstein equations, wave extraction techniques) are in use and have been shown to produce consistent results (eg. [4]).

Certain systematic errors, however, are difficult to estimate. In particular, current methods measure GWs at finite radii and extrapolate the results to infinity. This extrapolation has been identified as one of the largest remaining sources of systematic error within current extraction techniques, particularly during the merger and ring-down [5, 6]. Potential ambiguities arise particularly at small radii where gauge as well as nonlinear near-zone effects may dominate the expected polynomial falloff of the amplitude.

In this paper, we verify the extrapolation procedure for GWs by performing accurate wave extractions at large radii, out to $r = 1000M$ from the source (where M is the mass of the spacetime). The waveforms have been calculated using a new hybrid multi-patch/mesh-refinement algorithm, which allows for an efficient discretisation of the wave zone so that high accuracy can be obtained to large radii. We find that the measured waves between $r = 100M$ and $r = 1000M$ are convergent and of good enough quality to extrapolate the phase and amplitude accurately by low-order polynomial expansions. The measurements at $r = 1000M$ can be estimated to within 0.04% in amplitude and 0.001rad in phase, if the measurements out to $r = 600M$ are used in the extrapolation. This is true over the course of the evolution, including 8 orbits of inspiral, the merger, and ring-down. If only measurements within $r = 220M$ are used, as is common, then the errors increase by an order of magnitude.

Finally, we note that the gravitational radiation is normally associated with the leading order term in the falloff of the spacetime curvature. By the peeling theorem, we expect this to be a polynomial in $1/r$ whose leading coefficient is the Weyl component ψ_4. By measuring all of the Weyl curvature components, we have been able to establish their respective falloff rates, and verify that ψ_4 is indeed the leading order coefficient with the expected $1/r$ falloff rate. The exponents for the ψ_1 and ψ_0 components are less clear, however, and suggest that local gauge effects influence their computation.

II. Computational setup. – A key feature of the calculations performed here is the accuracy which we are able to achieve at large radii from the source through the use of a newly implemented numerical scheme. The code makes use of finite differences and standard mesh-refinement techniques, but incorporates the use of multiple grid patches to cover the spacetime with flexible adapted local coordinates. For the binary BH inspiral considered here, we consider two regions, depicted in Fig 1. In the near-zone region where the BHs orbit, we discretise the spacetime using standard Cartesian grids, applying 2:1 Berger-Oliger mesh refinement in order to increase the resolution around each body [7]. In the wave-zone, however, the dynamical fields are essentially radially propagating waves. We cover this zone with six overlapping patches, each of which incorporate a local radial coordinate r and transverse angular coordinates (ρ, σ). The use of six patches avoids the problem of a coordinate singularity on the axis of a single spherical-polar coordinate system, as well as providing a more uniform angular resolution over the sphere. The particular coordinates which we have implemented are the "inflated cube" coordinates, given explicitly in [8].

Derivatives on each grid are locally computed using standard finite differences at 8th-order. Data is passed between patches by interpolation, typically via centred 5th-order Lagrange polynomials. Each patch is surrounded by a boundary zone which is populated with data mapped from the neighbouring patch, so that derivatives can be calculated up to the patch edge without the need for off-centred stencils. A 4th-order Runge-Kutta integrator is used to evolve the solution.

We write the Einstein equations in the commonly used BSSNOK form [9, 10, 11, 12], adopting the particular variation proposed by [13], whereby the usual variable $\phi = \log\gamma/12$ is replaced by $w = \gamma^{-2}$ (with γ the 3-metric determinant). Gauges are the commonly used $1 + \log$ and $\tilde{\Gamma}$-driver conditions with advection terms [2, 3, 14].

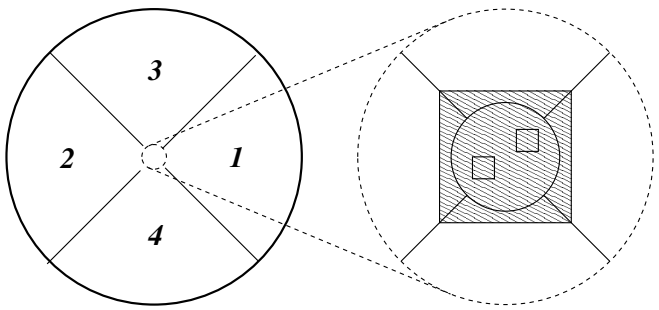

FIG. 1: Schematic depiction of the grid structure in the $z = 0$ plane. Four radial grids surround the equator. The right shows an expanded inset of the Cartesian grid (shaded) covering the near-zone around the individual BHs.

The GWs are measured by evaluating the Weyl curvature tensor components, $C_{\alpha\beta\gamma\delta}$, in a null frame $(\mathbf{l}, \mathbf{n}, \mathbf{m}, \bar{\mathbf{m}})$, oriented so that the outgoing vector, $\mathbf{l}$, points along the coordinate $\hat{\mathbf{r}}$ direction while the other vectors determine an orthonormal null frame in the local metric. The independent curvature components $\psi_0 \ldots \psi_4$ are determined by the standard projections [15]. The Weyl components are evaluated on spheres of fixed coordinate radius and projected onto a basis of spherical harmonics, ${}_{-2}Y_{lm}$. For binary black hole situation considered here, the dominant mode is $l = 2$, $m = 2$, which is used for the results presented here.

To establish the numerical accuracy, we have performed evolutions at three different resolutions, and find that the results converge at 4th-order during the merger, and close to 8th-order during the inspiral, in both amplitude and phase. (A more complete description of the code implementation and tests will be given elsewhere [16].) Here we present results based on the highest resolution evolved, for which the spatial resolution for all of the GW measurements is uniformly $h_r = 0.64M$ in the radial direction, and $h_\perp \simeq 3^\circ$ in the angular directions. GW measurements are taken every $0.144M$.

III. Extrapolation of waveforms. – We have evolved an equal-mass, non-spinning binary from separation $d/M = 11.0$ through approximately 8 orbits (a physical time of around $1360M$), merger and ring-down. The masses of the punctures are set to $m = (0.4872)$ and are initially placed on the x-axis with momenta $p = (\pm 0.0903, \mp 0.000728, 0)$, giving the initial slice an ADM mass $M = 0.99052$. These initial data parameters were determined using a post-Newtonian evolution from large initial separation, following the procedure outlined in [17], with the conservative part of the Hamiltonian accurate to 3PN and radiation-reaction to 3.5PN, and determine orbits with eccentricity less than 0.2%.

We measure the Weyl components $\psi_0 \ldots \psi_4$ every $20M$ from $r = 100M$ to $300M$, then at $400M, 500M, 600M$ and $1000M$. The radial grid structure in the wave zone allows us to extend the outer boundary of the grid at relatively little cost compared to Cartesian codes. For the runs presented here, it is placed at $r = 3600M$ with a resolution of $dr = 2.56M$ at the outer boundary so that the $l = 2$, $m = 2$ mode is reasonably well resolved throughout the grid. This allows for $2600M$ of evolution time before a physical or constraint violating mode traveling at the speed of light can reach the outermost detector at $r = 1000M$. That is, the outer boundary is effectively causally disconnected from the wave measurements presented in this paper.

The Weyl components $\psi_j = A_j e^{i\phi_j}$ are assumed to fall-off as a function of radius according to

$$A_j(r, t^*) = \sum_{i=0}^{n_A} \frac{A_j^{(i)}(t^*)}{r^i}, \qquad \phi_j(r, t^*) = \sum_{i=0}^{n_\phi} \frac{\phi_j^{(i)}(t^*)}{r^i}. \tag{1}$$

The r coordinate is that of the simulation coordinates, which we find to differ by at most 0.1% from the areal radius. The GWs are expressed in terms of the retarded time $t^* = t - r^*$ where t is the coordinate time and $r^* = r + 2M \ln[r/(2M) - 1]$ is the tortoise coordinate [5]. We do not offset the retarded time to align the peaks of the waveforms.

It is generally difficult to estimate the error incurred when extrapolating. Given the data at $r = 1000M$, we can attempt to gauge an optimal choice of extrapolation parameters by attempting to estimate this data from the measurements at smaller radii. As test cases, we construct extrapolations using four different sets of radii, $e_1 \in \{100M, 200M\}$, $e_2 \in \{160M, 280M\}$, $e_3 \in \{200M, 300M\}$ and $e_4 \in \{260M, 600M\}$. Each of these incorporates 6 data points, which over-determines low-order polynomials. We evaluate the extrapolation coefficients by a least-squares fit to these points, which can be important in removing spurious oscillations that may arise fitting high-order polynomials to noisy data.

Fitting the amplitude using various polynomial orders, n_A, suggests that in all cases $n_A = 3$ is optimal in predicting the amplitude of the measured wave at $r = 1000M$, with an error of approximately 0.02% for e_4 and 0.2% for e_1. For the phase, we find that $n_\phi = 3$ minimises the error, at 6×10^{-4}rad and 5×10^{-3}rad for e_4 and e_1, respectively. In both amplitude and phase, we note that the error is reduced significantly if the outermost data e_4 is used. In Fig. 2 we display the error in estimating the $r = 1000M$ data using each of the extrapolations at the optimal order. The maximum errors in both amplitude and phase tend to occur during the late inspiral ($t^* = -200M$ to $t^* = 0M$) and ring-down, although there is no sign of a rapid growth of error during this phase.

The corresponding extrapolations to $r \to \infty$ shows very similar behaviour. In Fig. 3, we have compared each of the extrapolations with an extrapolation obtained by including the $r = 1000M$ data ($e_5 \in \{280M, 1000M\}$), evaluated at $r \to \infty$. The outermost extrapolations differ by at most $\Delta A = 0.03\%$ and $\delta\phi = 0.003$rad over the course of the evolution.

IV. Peeling properties. – The interpretation of ψ_4 as the radiated gravitational energy is a consequence of the "peeling" property, which states that for asymptotically flat spacetimes at large radii, the Weyl curvature tensor can be represented

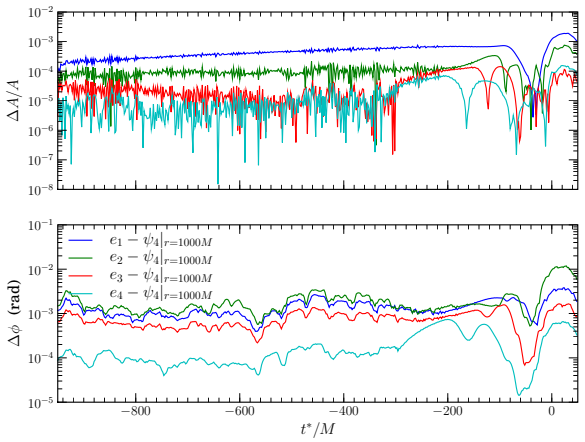

FIG. 2: Error in the extrapolated amplitude (top panel) and phase (bottom panel) of the $\ell = 2, m = 2$ component of ψ_4 at $r = 1000M$ as computed by extrapolations $e_1 \ldots e_4$ (defined in the text).

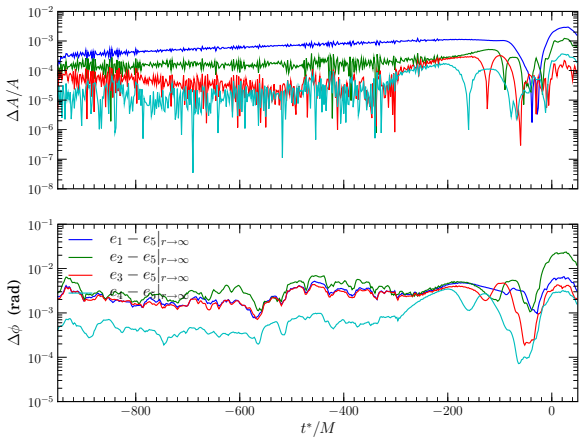

FIG. 3: Differences between the $r \leq 600M$ extrapolations with an extrapolation including $r = 1000M$ data (e_5) evaluated in the limit $r \to \infty$.

schematically as

$$C_{\alpha\beta\gamma\delta} \simeq \frac{\psi_4}{r} + \frac{\psi_3}{r^2} + \frac{\psi_2}{r^3} + \frac{\psi_1}{r^4} + \frac{\psi_0}{r^5} + O(1/r^6). \quad (2)$$

That is, each component of the Weyl tensor falls off at a known fixed rate, and at large radii, ψ_4 is the dominant component. At future null infinity, $\mathcal{J}^+$, it can be related to $\dot{M}$, the change in energy of the spacetime. We note, however, that the peeling theorem involves a number of restrictions on the asymptotic form of the spacetime, and the coordinates which are used there. A rigorous connection between finite radius measurements and the asymptotic properties of the spacetime at $\mathcal{J}^+$ is difficult to make.

Given the importance of the falloff of the curvature in the identification of ψ_4 with the GW, it is useful to examine the behaviour of the other Weyl components measured by the simulation. In Fig. 4, we have plotted their falloff as a function of coordinate radius. The time series data for each component is mapped to a scalar by integrating the amplitude over the interval $t \in [-800M, 50M]$. (Alternatively, one could obtain a scalar by taking the measurements at a point such as the waveform peak. A similar plot results, but the averaging effect of the integral reduces local noise slightly.)

For the cases of ψ_4 and ψ_3, we find that a straight line can be fitted to each of the components, indicating a consistent exponent, with measured values of -0.99 and -1.99 respectively, and a rather good agreement with Eq. (2). Due to its small amplitude, the ψ_2 measurement is dominated by numerical noise beyond a certain radius (clear from examination of the time-series data), and as a result, the curve veers from a straight line. However, if we fit a straight line to the five data points from $r \leq 200M$, we find an exponent, -2.99, again agreeing well with the expectation.

The ψ_1 and ψ_0 components present an interesting situation. Particularly in the case of ψ_0, the amplitude is large enough that a clear signal is present (of almost of the same amplitude as ψ_3). The falloff, however, is of order -2.00, rather than the -5 which the peeling theorem requires. Further, we note that the mode propagates outwards with a peak coincident with that of ψ_4, in contrast to the interpretation of ψ_0 as an "ingoing" component of radiation.

A possible explanation is that metric perturbations cause oscillations in the frame in which the components are measured. As described above, we define the null frame only with reference to the local space and time coordinates. Attempts to modify the falloff of ψ_0 via frame rotations (spin-boosts and null rotations) did not preserve the falloff of the other components. However, other gauge effects are likely present. We note that measurements are taken on spheres defined by the grid coordinates. The areal radius of these spheres exhibits small (on the order of 0.1%) oscillations in the $\ell = 2$, $m = 2$ mode. The finite-radius ψ_4 measurement is known to be susceptible to pure gauge effects such as the presence of a nonzero shift vector, which can produce spurious GW signals in static spacetimes [18]. Though these effects are small, so are the values of ψ_1 and ψ_0 and thus correspondingly sensitive compared to that of the dominant component.

V. Discussion. – We have demonstrated a number of features related to the measurement of GWs at finite radius. Our results suggest that polynomial extrapolation of the ψ_4 component from small radii can provide an accurate model for estimating the measurements at larger radii. Data measured within $r = 200M$ of the source have an error in amplitude and phase of $\Delta A \simeq 0.2\%$ and $\Delta\phi \simeq 5 \times 10^{-3}$rad throughout the evolution (including merger and ring-down) compared to the measurement at $r = 1000M$. This provides an important check on numerical relativity measurements, which typically extrapolate from $r < 200M$. Larger radius measurements do, however, improve the extrapolation, and errors can be reduced by a further order of magnitude if data to $r = 600M$ is included. We also note that while ψ_4 is dominated by the

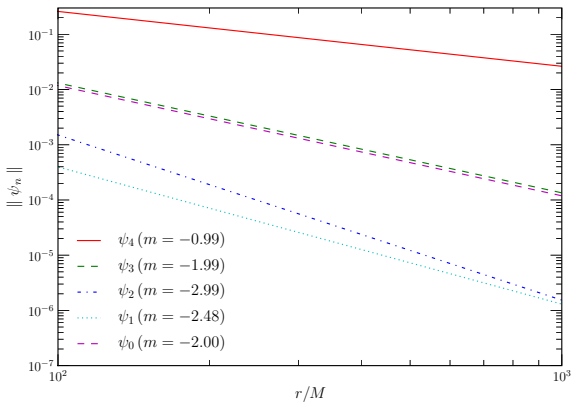

FIG. 4: The radial falloff of the Weyl components. Lines are linear least-squares fits to all of the points of ψ_0, ψ_3, and ψ_4, and the $r \leq 200M$ points for ψ_1 and ψ_2. Measured slopes are listed in the legend.

$1/r$ term beyond $r = 300M$, at smaller radii the higher order terms have a much larger contribution.

While the falloff of ψ_4 is the leading order contribution to the curvature as expected, the results of Fig. 4 suggest that the picture may be more complicated for the other Weyl components, and that care should be taken in interpreting local variables according to their expected asymptotic properties. With respect to the peeling property, we note that the asymptotic evolution of generic initial data sets are likely to include polyhomogenous terms, and even the situation for Bowen-York data with linear momentum is not clear [19, 20]. While it seems most likely that the effect we have observed in ψ_0 and ψ_1 is related to gauge, this provides a strong caution regarding physical predictions based on these quantities. Alternative gauge conditions may alleviate (or exaggerate) the issues we have noted.

The mapping of finite radius results to asymptotic values at $\mathcal{J}^+$ needs to be considered with some care. While our results suggest that the procedure of extrapolation is self-consistent and can be used to estimate the results that would be obtained by direct measurement at large radii, they do not establish the identification of the extrapolated quantities with quantities that would be measured at $\mathcal{J}^+$. In a related paper [21], we have demonstrated that the extrapolation procedure does in fact reproduce results obtained at $\mathcal{J}^+$ to high accuracy, though a small systematic error does remain. A number of local corrections have been proposed to improve the rigor of ψ_4 measurements at finite radius (cf. [22, 23, 24]).

Finally, we note that our accurate measurements at $r = 1000M$ are a result of a new computational infrastructure making use of adapted coordinate grids in conjunction with a finite difference, moving-puncture scheme. This is the first demonstration that such methods can produce stable evolutions for dynamical spacetimes. The efficiency gains allow the wave zone to be covered with sufficient resolution to very large radii ($3600M$ in this case), which has been a crucial in reducing boundary errors.

Acknowledgments.– The authors are pleased to thank: Ian Hinder, Sascha Husa, Badri Krishnan, Philipp Moesta, Luciano Rezzolla, Juan Valiente-Kroon for their helpful input; the developers of Cactus [25] and Carpet [7] for providing an open and optimised computational infrastructure on which we have based our code; support from the DFG SFB/Transregio 7, the VESF, and by the NSF awards no. 0701566 *XiRel* and no. 0721915 *Alpaca*. Computations were performed at the AEI, at LSU, on LONI (numrel03), on the TeraGrid (TG-MCA02N014), and the Leibniz Rechenzentrum München (h0152).

[1] F. Pretorius, Phys. Rev. Lett. **95**, 121101 (2005).
[2] J. G. Baker, J. Centrella, D.-I. Choi, M. Koppitz, and J. van Meter, Phys. Rev. Lett. **96**, 111102 (2006).
[3] M. Campanelli, C. O. Lousto, P. Marronetti, and Y. Zlochower, Phys. Rev. Lett. **96**, 111101 (2006).
[4] M. Hannam et al., Phys. Rev. **D79**, 084025 (2009).
[5] M. A. Scheel et al., Phys. Rev. **D79**, 024003 (2009).
[6] M. Boyle and A. H. Mroue (2009).
[7] E. Schnetter, S. H. Hawley, and I. Hawke, Class. Quantum Grav. **21**, 1465 (2004).
[8] J. Thornburg, Class. Quantum Grav. **21**, 3665 (2004).
[9] T. Nakamura, K. Oohara, and Y. Kojima, Prog. Theor. Phys. Suppl. **90**, 1 (1987).
[10] M. Shibata and T. Nakamura, Phys. Rev. D **52**, 5428 (1995).
[11] T. W. Baumgarte and S. L. Shapiro, Phys. Rev. D **59**, 024007 (1998).
[12] M. Alcubierre, B. Brügmann, T. Dramlitsch, J. A. Font, P. Papadopoulos, E. Seidel, N. Stergioulas, and R. Takahashi, Phys. Rev. D **62**, 044034 (2000).
[13] P. Marronetti, W. Tichy, B. Bruegmann, J. Gonzalez, and U. Sperhake, Phys. Rev. **D77**, 064010 (2008).
[14] M. Alcubierre, B. Brügmann, P. Diener, M. Koppitz, D. Pollney, E. Seidel, and R. Takahashi, Phys. Rev. D **67**, 084023 (2003).
[15] E. T. Newman and R. Penrose, J. Math. Phys. **3**, 566 (1962), erratum in J. Math. Phys. 4, 998 (1963).
[16] D. Pollney, C. Reisswig, E. Schnetter, N. Dorband, and P. Diener (2009), submitted to PRL.
[17] S. Husa, M. Hannam, J. A. Gonzalez, U. Sperhake, and B. Bruegmann, Phys. Rev. **D77**, 044037 (2008).
[18] C. Reisswig, N. T. Bishop, D. Pollney, and B. Szilágyi (2009), in preparation.
[19] P. T. Chrusciel, M. A. H. MacCallum, and D. B. Singleton, Proc. Roy. Soc. Lond. **A436**, 299 (1992).
[20] J. A. Valiente Kroon, Class. Quant. Grav. **24**, 3037 (2007).
[21] C. Reisswig, N. T. Bishop, D. Pollney, and B. Szilagyi (2009).
[22] A. Nerozzi, Phys. Rev. **D75**, 104002 (2007).
[23] L. Lehner and O. M. Moreschi (2007).
[24] E. Deadman and J. M. Stewart, Class. Quant. Grav. **26**, 065008 (2009).
[25] T. Goodale, G. Allen, G. Lanfermann, J. Massó, T. Radke, E. Seidel, and J. Shalf, in *Vector and Parallel Processing – VECPAR'2002, 5th International Conference, Lecture Notes in Computer Science* (Springer, Berlin, 2003).